UNIVERSITÀ POLITECNICA DELLE MARCHE

FACOLTÀ DI INGEGNERIA

Corso di Laurea Magistrale in Ingegneria elettronica

PROGETTO DI LENTE A METAMATERIALI PER ANTENNE BOWTIE A 140 GHz

METAMATERIAL LENS DESIGN FOR BROADBAND BOWTIE ANTENNA AT 140 GHz

Relatore:
Chiar.mo/a
Prof. Luca Pierantoni

Tesi di Laurea di:
Gian Marco Zampa
S1092546

ANNO ACCADEMICO 2021/2022

Contents

Abstract

Questa tesi ha lo scopo di presentare il progetto di una lente a metamateriali che lavori a 140 GHz per un'antenna di tipo *bowtie*. Sebbene in letteratura esistano numerosi articoli che trattano di lenti per antenne, l'idea innovativa alla base di questo progetto è quella di realizzare un dispositivo che possa essere realizzato in tecnologia planare, tramite gli stessi processi produttivi con cui si realizza l'antenna stampata. Grazie all'utilizzo di metamateriali è stato possibile progettare una lente cilindirca ad indice di rifrazione variabile in silicio. Il profilo desiderato dell'indice di rifrazione si ottiene realizzando fori di dimensioni differenti nel cilindro di silicio. In questo modo, in base alla percentuale di aria e di silicio in ogni sezione della lente, l'onda elettromagnetica incidente osserverà un materiale con constante dielettrica di valore compreso tra quella dell'aria e quella del silicio. Ciò è possibile in quanto la dimensione dei fori è molto minore della lunghezza d'onda a 140 GHz. Anelli più esterni presentano fori più grandi mentre avvicinandosi al centro si hanno dimensioni minori. La presenza di un materiale con indice di rifrazione variabile fa sì che le onde elettromagnetiche che si propagano al suo interno si propaghino con velocità di gruppo differenti al variare della posizione. Ciò comporta che i raggi che si propagano negli strati più esterni (con indice minore) siano più veloci mentre quelli negli strati più interni più lenti. In questo modo si compensa la differenza di lunghezza del percorso andando di fatto a trasformare l'onda emessa dalla sorgente (antenna) in un'onda piana. Il progetto del dispositivo è stato effettuato utilizzando il simulatore COMSOL Multiphysics ®. Sono stati effettuati studi preliminari sull'antenna utilizzata e successivamente sull'antenna combinata con la lente, in questo modo è stato possibile confrontare i risultati verificando l'efficacia della lente. Il modello è stato realizzato tenendo conto dei vincoli di realizzazione della catena produttiva SiGe degli IHP, e l'antenna è provvista di una rete di adattamento che consente dopo la realizzazione del dispositivo di effettuare misurazioni che potranno validare i risultati delle simulazioni effettuate. La presenza della lente rende l'antenna *bowtie* molto più direttiva raggiungendo un guadagno effettivo di 11.02 dB, contro gli 1.89 dB dell'antenna da sola (nel guadagno sono comprese le perdite della rete di alimentazione e di disadattamento, nonché l'efficianza dell'antenna). L'aumento considerevole del guadagno comporta una leggera riduzione dell'efficienza totale che passa dall'85% all'82%. Rispetto ai 20 GHz della bowtie la banda del modelo con la lente risulta ridotta con un return loss sotto i -10 dB da 135 GHz a 149 GHz, ovvero per 14 GHz (il 10% di banda in proporzione alla frequenza di centrobanda). Nonostante la riduzione della banda e del guadagno (che cala al di fuori dei 140 GHz, rimandendo comunque al di sopra dei 5 dB) il modello finale risulta funzionare correttamente a larga banda con prestazioni migliori dell'antenna singola.

Introduction

Metamaterials have become an hot topic in recent years due to the vast application possibilities. These materials can achieve some physical properties that do not exist in nature, allowing to design and realize better devices and systems. The study of metamaterials opens up various researching fields especially in antenna applications. Metamaterials allow to realize antennas with higher gain, wider bandwitdth or lower dimensions. Due to a wider band necessity for the fifth mobile network generation, mm-wave have been used. Using higher frequencies requires solving propagation problems due to the high path attenuation and the wide number of users in a same spot. The next mobile generation has the focus to use even higher frequencies hitting hundreds of GHz. A possible solution is to use lenses to improve antennas directivity and gain in order to achieve a lower bit error rate in communication. The issues of using lenses is the difficulty of realization curved silicon surfaces and the impossibility to use the actual SiGe productive chain. Gradient index lenses can solve the first problem not requiring a particular geometrical profile but still can not be realized in the same wafer of the antenna. Metamaterials can be used to realize GRIN lenses with a planar surface. The focus of this thesis is to design a cylindrical lens made of silicon. The lens should work for a bowtie antenna at 140 GHz. The idea is to realize a silicon cylinder with holes of different sizes along the radial direction. Holes must be smaller than the wavelength in order for an electromagnetic wave to see a homogeneous dielectric. The dielectric permittivity therefore decreases as the size of the holes increase. Such lenses could be printed in the same wafer of the antenna allowing the device to be realized in a productive chain. This kind of lens can therefore be used for many different kind of printed antenna, allowing to achieve higher gains necessary for high frequency applications. In this thesis the device composed by the antenna combined with the metamaterial lens is modeled using COMSOL Multiphysics ®. All the dimensions are defined considering the IHP - Innovations for High Performance Microelectronics technology in order to design a model that could be physically realized. The bowtie antenna also presents a feeding network with pads used to do measurement of the realized prototype. After few chapters explaining the basic theory of metamaterials and gradient index lenses, the thesis presents the models used to realize the final device design and the results of the simulations done.

Chapter 1

Metamaterials

1.1 General classification

A metamaterial is an artificial material designed to have physical properties that do not exist in nature. These properties are obtained by arranging specific microstructures called "atoms" or cells. Considering the electromagnetic properties (ε and μ), metamaterials can be divided in four different groups:

1. Double positive (DPS), materials that have $\varepsilon > 0$ and $\mu > 0$. This group represents the major part of the existing natural material.

2. Epsilon negative (ENG), materials that have $\varepsilon < 0$ and $\mu > 0$. This group is represented by plasmas.

3. Double negative (DNG), materials that have $\varepsilon < 0$ and $\mu < 0$. This group does not exist in nature and it is completely artificial.

4. Mu negative (MNG), materials that have $\varepsilon > 0$ and $\mu < 0$. This group is represented by ferrites.

Figure 1.1 shows the material classification. The refractive index of a material $n = \sqrt{\varepsilon_r \mu_r}$, depending on the type of material, could be both real or imaginary and positive or negative. In DPS and DNG materials the refraction index is real and all the waves can propagate, in ENG and MNG evanescent waves can be found because of the imaginary refraction index.

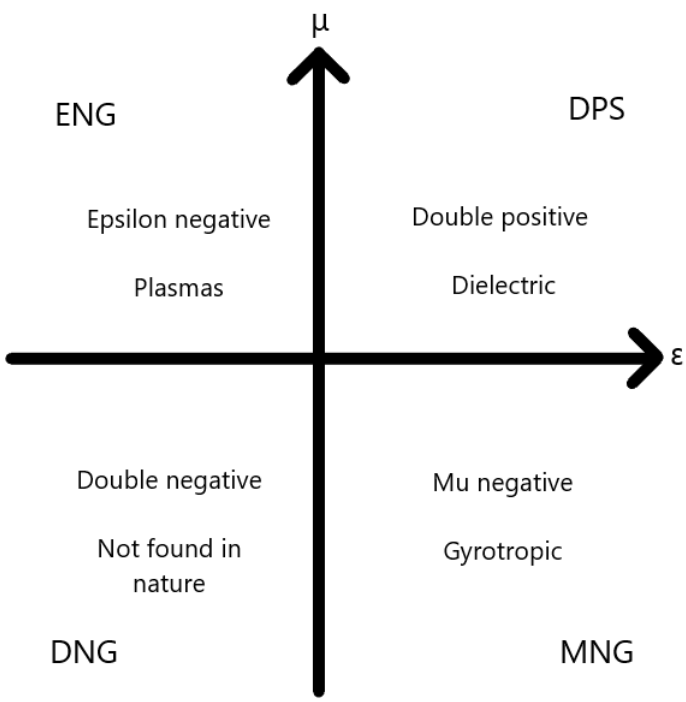

Figure 1.1: Metamaterial classification considering electromagnetic properties

1.2 ENG metamaterials

The dielectric permittivity of a plasma varies in frequency as shown in equation 1.1.

$$\varepsilon_r = 1 - \frac{(\omega_p^2)}{\omega^2} \tag{1.1}$$

The permittivity is positive for waves propagating above the plasma frequency (ω_p) and negative below. A simple design for an ENG metamaterial is a matrix of cells containing a thin metal wire as shown in figure 1.2. This lattice behaves as a high pass filter for an incident plane wave with an electric field parallel to the wires. The propagation is similar to the propagation in a plasma medium. The ENG metamaterial presents a plasma frequency that depends on the wires radius and the distance between two adjacent conductors (lattice constant).

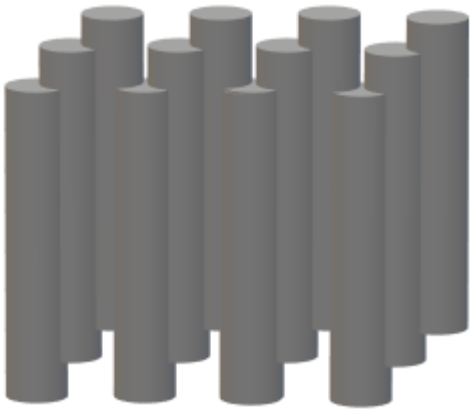

Figure 1.2: Lattice of thin metal wires working as a ENG metamaterial

This behavior can be achieved only if the lattice constant is much smaller than the wavelength.

1.3 MNG metamaterials

The most popular cell that behaves as MNG material is the split ring resonator (SRR). The cell is composed by two concentric (circular or square) rings separated by a gap. Each ring has a narrow slot that faces opposite directions (180°) as shown in figure 1.3.

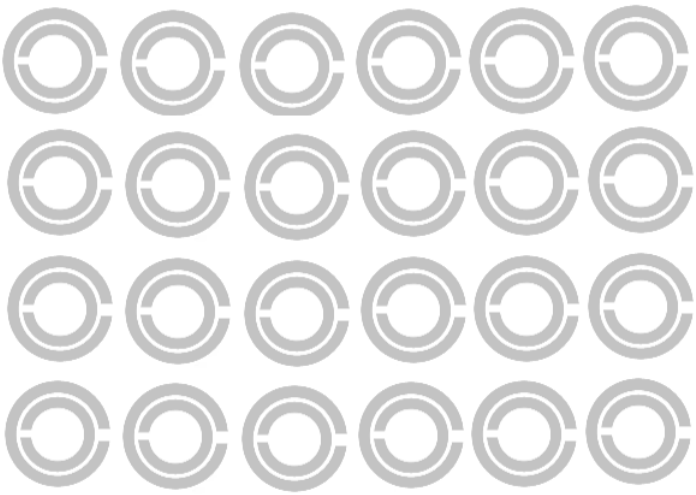

Figure 1.3: Lattice of split ring resonators working as a MNG metamaterial

The rings work as an inductor and the gap behave like a capacitor. This cell behaves as an LC resonant circuit for a normal incident plane wave. The effective permeability of MNG lossless material realized by spiral ring resonators is given by equation:

$$\mu_{eff} = 1 - \frac{\omega_{mp}^2 - \omega_0^2}{\omega^2 - \omega_0^2} \tag{1.2}$$

where ω_0 is the resonation frequency and ω_{mp} is the magnetic equivalent plasma frequency. The permeability is negative for waves propagating between ω_0 and $_{mp}$ and positive above. This behavior can be achieved only if the spiral ring resonator dimension is much smaller than the wavelength.

1.4 DNG metamaterials

A DNG material could be obtained combining the ENG and the MNG cells proposed in section 1.2 and 1.3. This material presents a negative refractive index value.

$$n = \sqrt{\varepsilon_r}\sqrt{\mu_r} = -\sqrt{|\varepsilon_r|}\sqrt{|\mu_r|} = -|n| \tag{1.3}$$

This is possible if there is at least an interval of frequencies where there is a superposition of the ENG and MNG properties. The permittivity and the permeability can be described in frequency by a lossless Drude model as follow.

$$\varepsilon_{eff} = 1 - (\omega_{pe}^2)/\omega^2 \tag{1.4}$$

$$\mu_{eff} = 1 - (\omega_{pm}^2)/\omega^2 \tag{1.5}$$

If ω is lower than ω_{pe} and ω_{pm}, then the permittivity and permeability values are negative. In DNG material particular phenomenon occurs such as the negative refraction or the backward waves propagation. Further explanations can be found at [1].

1.4.1 Backward waves

Suppose an x-polarized plane electromagnetic wave propagating in a dielectric medium along the z axis. The phasors fields are the following:

$$\overline{E} = E_0 e^{-jkz}\widehat{x} \tag{1.6}$$

$$\overline{H} = H_0 e^{-jkz}\widehat{y} \tag{1.7}$$

The wavenumbers, obtained by the plane wave dispersion relation ($k^2 = \omega^2\varepsilon_r\mu_r$), have the following values respectively in a DPS and in a DNG material:

$$k^{DPS} = \sqrt{(\omega^2\varepsilon_r^{DPS}\mu_r^{DPS})} = \omega|n| \tag{1.8}$$

$$k^{DNG} = -\sqrt{(\omega^2\varepsilon_r^{DNG}\mu_r^{DNG})} = -\omega|n| \tag{1.9}$$

The plane wave impedance is the same in both DPS and DNG material and it is given by equation 1.10:

$$\eta^{DPS} = \eta^{DNG} = \eta = \frac{E_0}{H_0} = \frac{k}{\omega\varepsilon_0\varepsilon_r} = \sqrt{\frac{\varepsilon_0\varepsilon_r}{\mu_0\mu_r}} = \eta_0\sqrt{\frac{\varepsilon_r}{\mu_r}} \tag{1.10}$$

The Poynting vector calculated in both media is obtained by the relation below:

$$\overline{P} = \frac{1}{2}\Re[E \times H^\star] = \frac{E_0^2}{2\Re[\eta^\star]}e^{-2\Im[k]z}\widehat{z} \tag{1.11}$$

The propagation constants have opposite sign in the two media. In the DNG material the wave phase shifts backward as if the source was in the opposite direction of the incident wave. The Poynting vector maintains the same direction in both media because of the causality principle. This phenomenon is called backward wave propagation. An exhaustive exposition can be found at [2]

1.5 Gradient index metamterials (GRIN)

Gradient index material are mediums which have a variable refractive index. These are often used in optics in order to create lenses with flat surfaces. The refraction gradient could be spherical, axial or radial.

A GRIN material can be realized using metamaterials. As exposed in section 2 a split ring resonator generates a frequency variable magnetic permeability and therefore a variable refractive index. Different ring designs have different resonant frequencies and then different refractive index values at the same frequency. The desired gradient profile can be achieved using different SRRs. Details of the metamaterial design can be found at [3]. In this thesis a different GRIN metamaterial is used. The cell is made of a perforated dielectric. An electromagnetic wave sees a dielectric with a permittivity value that depends on the hole surface to cell surface ratio. In particular the value is in range $[\varepsilon_{air}, \varepsilon_{dielectric}]$. This is only possible if the wavelength

is various times the hole dimension. In order to obtain the desired permittivity value, the square hole dimension can be found using equation 1.12:

$$\frac{d_{hole}}{w_{cell}} = 1 - \frac{\varepsilon_{desired}}{\varepsilon_{dielectric} - 1} \tag{1.12}$$

This equation can be obtained by simple geometric considerations, considering the ratio between the hole surface and cell surface.

1.6 Antenna application of metamaterials

A large number of metamaterial applications to antenna design are presented in literature. Metamaterial can improve radiation properties, such as bandwidth or gain, or geometric properties allowing to design smaller antennas. Metamaterial can be used as the antenna environment or as part of the antenna structure. Lenses realized with GRIN metamaterials are an example of the use of metamaterials as part of the antenna structure to improve gain. Antenna size can be reduced thanks to high permeability metamaterials. The wavelength at the working frequency in such materials is lower than normal dielectrics as shown in equation. A patch antenna placed in a such substrate has to be smaller than a regular patch due to its resonance at $\lambda/2$.

$$\lambda = \frac{\lambda_0}{\sqrt{\varepsilon_r \mu_r}} \tag{1.13}$$

Many other examples of antenna application can be found in [4] and [5]

Chapter 2

Gradient index lenses

Contents

Lenses collimate divergent energy to prevent it from spreading in undesired directions. A lens can be combined with different kind of antennas depending on application, going from parabolic reflector to printed antennas. Lenses can be realized using homogeneous or inhomogeneous dielectric. Although the firsts are the most common in MM-wave applications the seconds present a peculiar behavior and can be realized using flat surfaces. In classical homogenous lenses a proper geometrical configuration transforms divergent energy into plane waves. Gradient index lenses collimate the radiation using a variation of the refractive index of the material instead. This allows to produce lenses with flat surfaces using spheres or cylinders. Traditional lenses can be converted in gradient index lenses using transformation optics optics as exposed in [6] and [7]. GRIN lenses may present a symmetry that can be either spherical, radial (cylindrical) or axial. This kind of lenses is more difficult to physically realize due to material inhomogeneity. In recent years, the development of metamaterials research has allowed to design materials with the desired dielectric permittivity properties. Gradient index metamaterials open up a whole area of research, creating several opportunities. Some of the GRIN lenses well known in literature are presented in the following sections.

2.1 Spherical symmetry GRIN lenses

A spherical symmetry GRIN lens presents a refractive index in the form of equation 2.1

$$n = n(r) \tag{2.1}$$

Where $r^2 = x^2 + y^2 + z^2$ is the radius in spherical coordinates with the origin in the center of symmetry. The refraction of an electromagnetic ray that pass through a spherical symmetry lens can be calculated analytically as shown in [8] and [9].

2.1.1 Maxwell fish-eye lens

A Maxwell fish-eye (MFE) lens makes the energy of a point source converge into a focus point in the opposite side of the lens. These lenses are therefore omnidirectional. Due to the symmetry of the structure, at the center of the lens the wave is converted into a plane wave. Hence, half Maxwell fish-eye lens (HMFE) makes the radiation of a point source highly directive. An MFE lens is a spherical lens with refractive index that varies with the radius as in equation 2.2

$$n(r) = \frac{n_0}{1 + \left(\frac{r}{R}\right)^2} \tag{2.2}$$

Where n_0 is the refractive index at the center of the lens, R is the radius of the lens and r is the distance from the center of the lens.

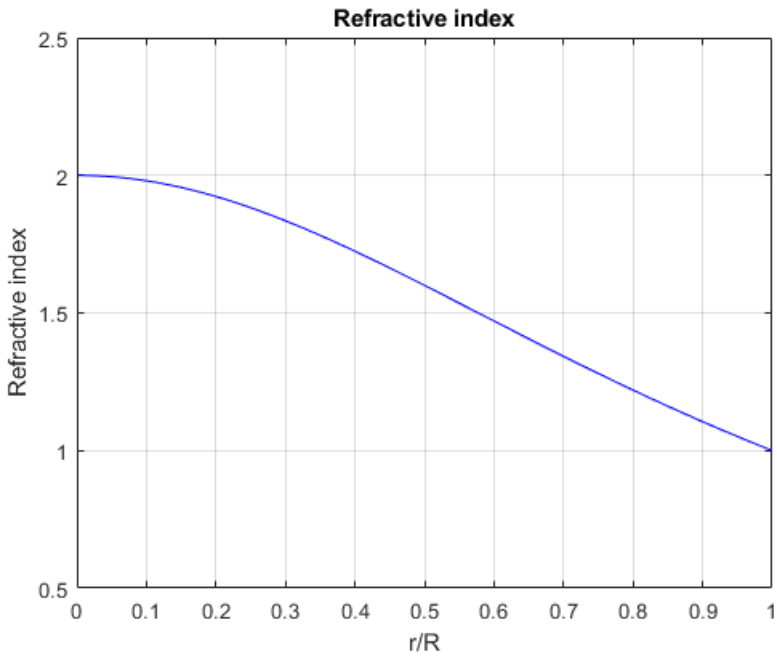

Figure 2.1: Refractive index of a Maxwell fish-eye lens

A detailed analysis of the MFE lens can be found in [**GRINopt**] and an implementation in [10].

2.1.2 Luneburg lens

A Luneburg lens is a sphere composed by an inhomogeneous dielectric with a refractive index that varies with the radius as in equation 2.3

$$n(r) = \sqrt{2 - \left(\frac{r}{R}\right)^2} \tag{2.3}$$

The Luneburg lens converts the energy of a point source to a flat wave. This effect makes the radiation highly directive. The electric profile of a Luneburg lens is shown in figure 2.2

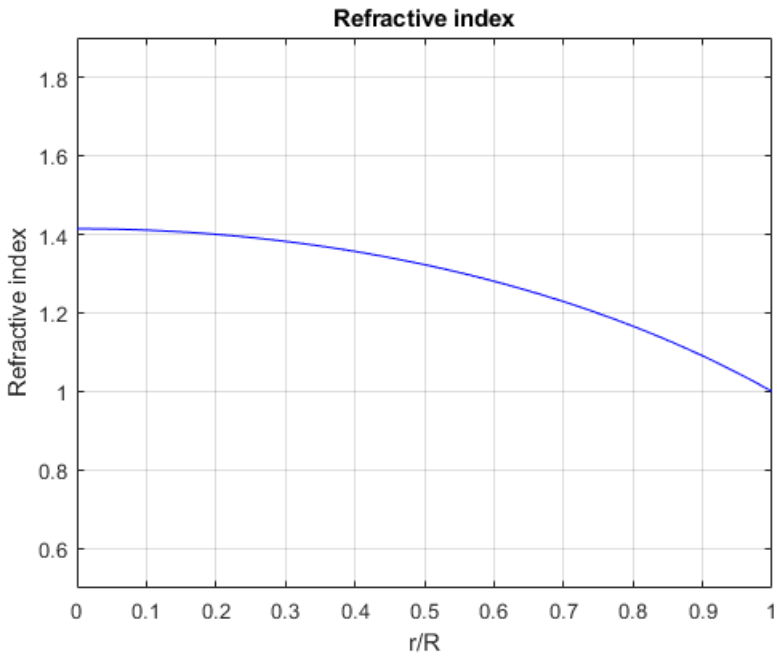

Figure 2.2: Refractive index of a Luneburg lens

This lens was first introduced by Luneburg in [9]. A metamaterial implementation can be found in [11].

2.1.3 Generalized Eaton lens

Another kind of lens is the Eaton one. These lenses enable to control the output direction of the incident radiation through refraction. Three classical configurations have been studied in literature:

- the *Right bender* with a refraction angle of 90°;
- the *Retroreflector* with a refraction angle of 180°;
- the *Time delayer* with a refraction angle of 360°.

As presented in [12], the refractive index of the generalized Eaton lens can be obtained by equation 2.4.

$$n^{\frac{\pi}{\theta}} = \frac{R}{nr + \sqrt{\frac{R}{n^2 r^2} - 1}} \tag{2.4}$$

Where θ is the desired refraction angle, R is the radius of the lens and r is the distance from the center of the lens. As shown this equation is not analytic and it presents a singularity in $r = 0$. The refractive index value is infinite in the center of the lens.

2.2 Radial symmetry GRIN lens

A radial symmetry GRIN lens has a refractive index that can be easily written using cylindrical coordinates. Some basic equations which describe the wave propagation in such mediums can be found in [8]. These equations cannot be integrated analytically except in particular cases. The lens designed in this thesis belongs to this group and has a dielectric permittivity between ε_{max} and ε_{min} as in equation.

$$\varepsilon_r(r) = \varepsilon_{min} + (\varepsilon_{max} - \varepsilon_{min}) \left(\frac{r}{R}\right)^{\nu} \tag{2.5}$$

For non-magnetic materials the refractive index corresponds to the square root of the permittivity value. Other solutions are presented in literature as the ones exposed in [13] and [14]

Chapter 3

Models implementation

Contents

3.1 IHP Technology stack

Figure 3.1 shows the utilized SiGe technology stack. The acronym TM stand for "top metal", TV stand for "top via", M for "metal" and V for "via".

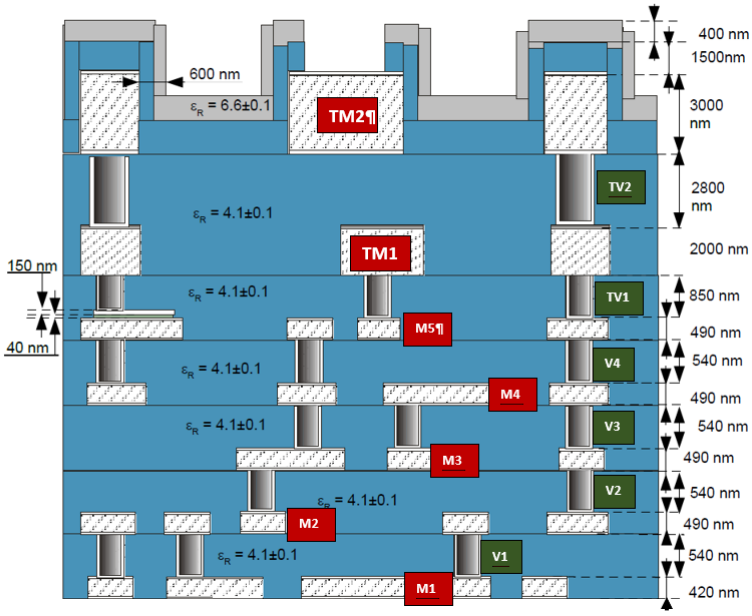

Figure 3.1: IHP SiGe technology stack

The blue regions represent the dielectric substrate with a relative dielectric permittivity of 4.1. The grey region on top represent an insulator with a relative dielectric permittivity of 6.6. The regions with a red tag can be used to print metal surfaces. The ones with a green tag can be used to create connection vias through different metal layers.

Only TM2, TV2 and TM1 layers are utilized in these models. These layers have a conductivity respectively of $\sigma_{TM2} = 3.03 \times 10^7 S/m$, $\sigma_{TV2} = 3.143 \times 10^6 S/m$ and $\sigma_{TM1} = 2.78 \times 10^7 S/m$. In TM2 and TM1 layers the minimum track width realizable is respectively of 2 m and 1.64 m, so does the minimum space between different metal tracks.

The silicon wafer substrate has an $\varepsilon_r = 11.7$ and a high resistivity $\sigma_{Si} = 2.5 \times 10^{-2} S/m$. The wafer thickness is 7 mm and two wafers can be pasted in order to achieve a double thickness.

All these models are designed using the IHP technology, considering the physical realizability constraints.

3.2 Simulated physics

All the models are implemented in Comsol using the electromagnetic waves, frequency domain module. This module allows to solve the phasors Maxwell equations in the model and to compute some fundamental parameters in RF and antennae simulations. Those are the main

parameters:

- Directivity (D), radiated power to isotropic equivalent radiated power ratio;
- Gain (G), same as the directivity considering the isotropic power equals to the power in input at the antenna port;
- Realized Gain (G_r), same as the directivity considering the isotropic power equals to the power in input at the feed port;
- Radiation Efficiency (e_r), radiated power to input power at the antenna port ratio (equivalent to the gain to directivity ratio);
- Total Efficiency (e_{tot}), radiated power to input at the feed port ratio (equivalent to the realized gain to directivity ratio);
- Return Loss (L_r), reflected power at the port (s_{11} coefficient in the S-matrix).

Those parameters are obtained by a far field evaluation. The far field is calculated through a spherical surface surrounding the substrate. The sphere is made of air and it is surrounded by another sphere at $\lambda/2$ distance which implements a perfectly matched layer condition (the PML condition is necessary in order to remove boundary reflections).

3.3 Antenna models

3.3.1 Bowtie antenna

The first model implements in COMSOL Multiphysics a bowtie antenna to work at 140 GHz without a feeding network as it shown in figure 3.2.

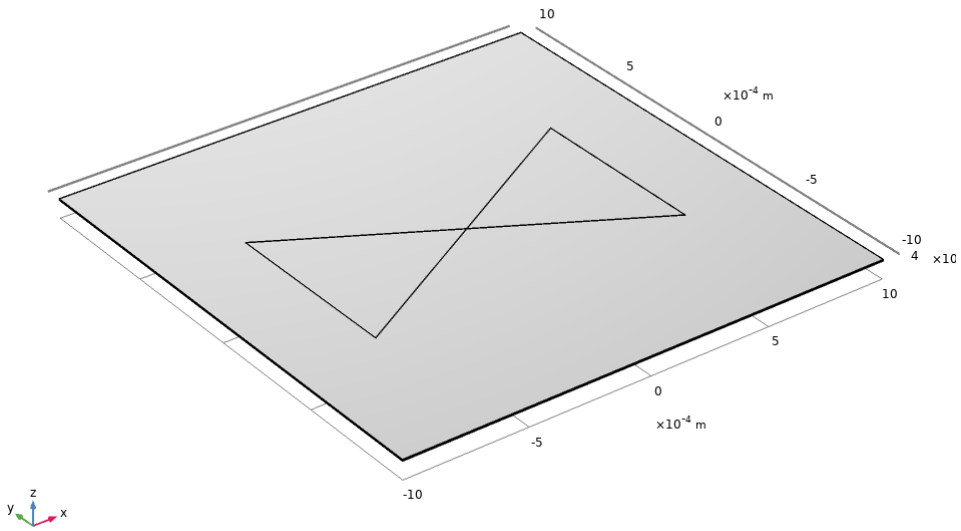

Figure 3.2: Bowtie antenna model in COMSOL

The port is placed in between the triangle patches and it feed the antenna with an x-oriented wave. The following parameters, obtained by a parametric sweep, are used to maximize the radiated power at working frequency (140 GHz).

Parameters	**Value**
Major base	750 μm
Minor base	3 μm
Height	625 μm
Gap width	5 μm

A trapezium is used instead of the triangle because a sharp corner is hard to physically realize with precision due to technology constraints. The substrate and metal layers thickness are imposed by the IHP technology stack discussed in section 3.1.

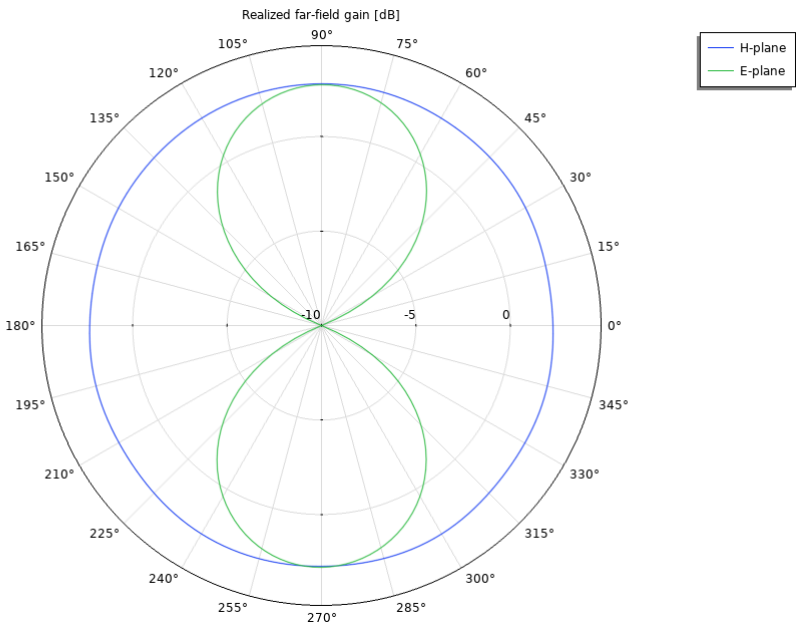

Figure 3.3: Realized far-field gain (E and H planes)

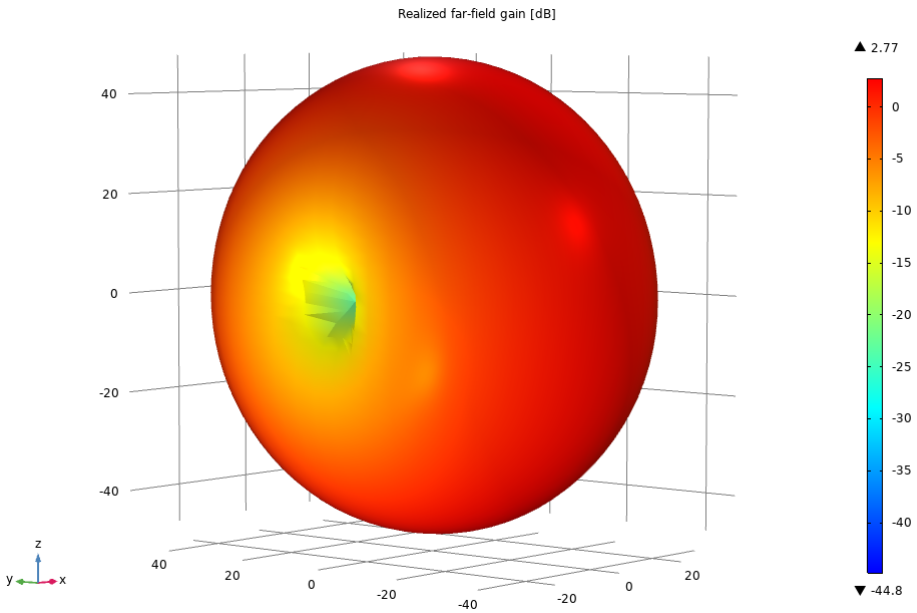

Figure 3.4: Realized far-field gain (3D)

The radiation patterns shown in figures 3.3 and 3.4 are the ideal result for a bowtie but they are also a good reference to compare with a more realistic antenna implementation.

3.3.2 Bowtie antenna with a feeding network

The bowtie antenna needs a differential feed to be excited. A microstrip port is usually used to connect the printed antenna to the measure instrument. Hence it is necessary to design a transition between an unbalanced microstrip line and a balanced one. Figure 3.5 shows the feeding network front and back suggested design. The blue colored selection represent the aluminium track.

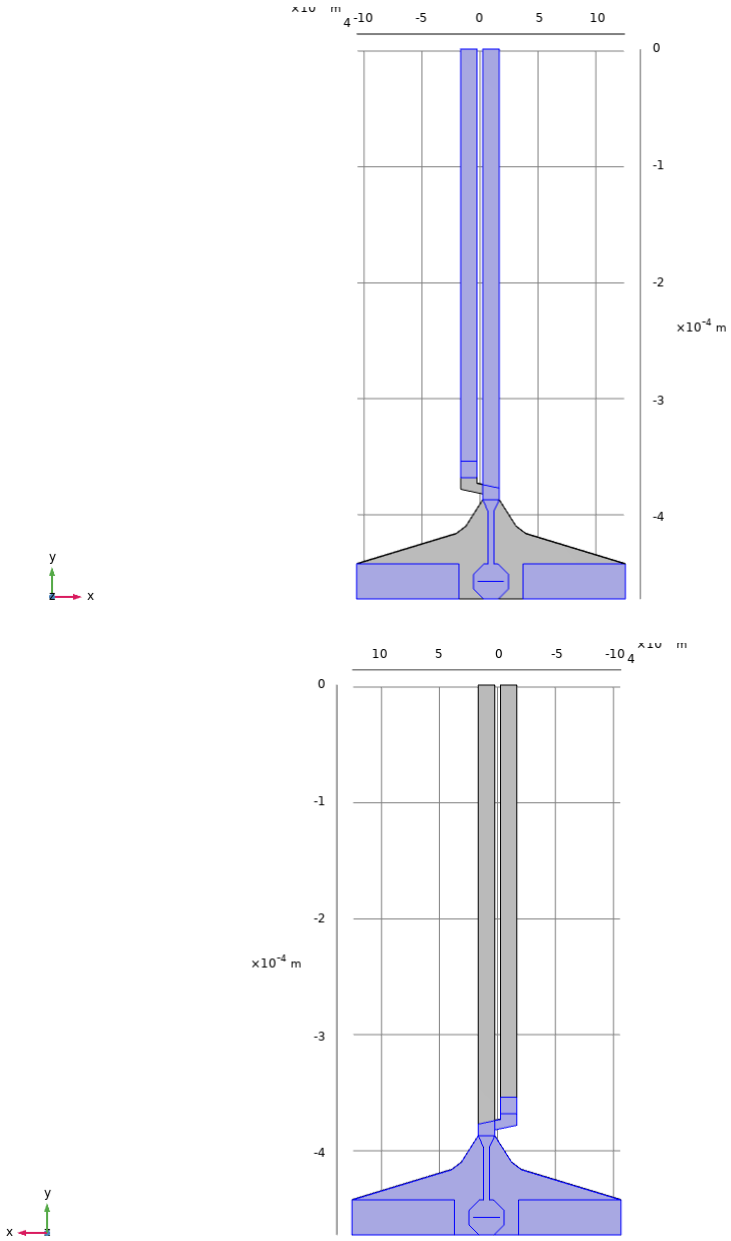

Figure 3.5: Feeding network front and back

Two rectangles on the bottom work as ground pads connecting the ground to the conductor on the bottom side with an aluminium via. The ground plane narrows and connects to one of

the signal lines on the top side of the substrate, thanks to a balun network. The signal pad (the octagon on the bottom) is connected to one of the signal lines through an adapter section. The balanced line is directly connected to the bowtie antenna.

The model of the antenna combined with the feeding network is shown in figure 3.6.

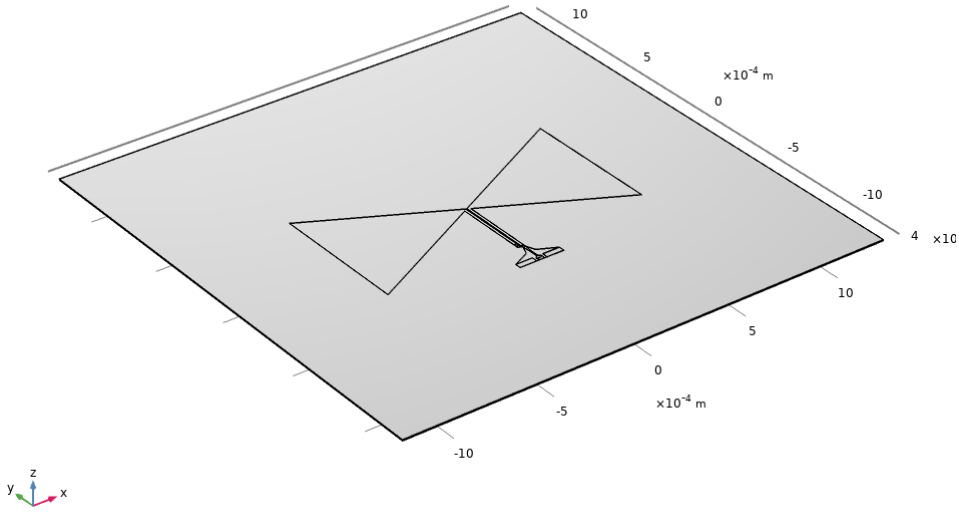

Figure 3.6: Bowtie antenna combined with the feeding network model in COMSOL

The feed presence unbalances the bowtie because the output impedance needs to match exactly the antenna impedance. This requires an optimization process. The matching is obtained by evaluating and minimizing the return loss at the entrance port through a parametric sweep. The degree of freedom considered are the bowtie parameters, the feed line length and width, the balun length and the input microstrip width. The following parameters guarantee the solution to be matched.

Parameters	**Value**
Bowtie major base	708 μm
Bowtie minor base	3 μm
Bowtie height	667 μm
Bowtie gap width	5 μm
Feed length	377 μm
Feed width	14 μm
Balun length	135 μm
Microstrip width	5 μm

Figures 3.7 and 3.8 show how the radiation pattern change from the bowtie alone simulation.

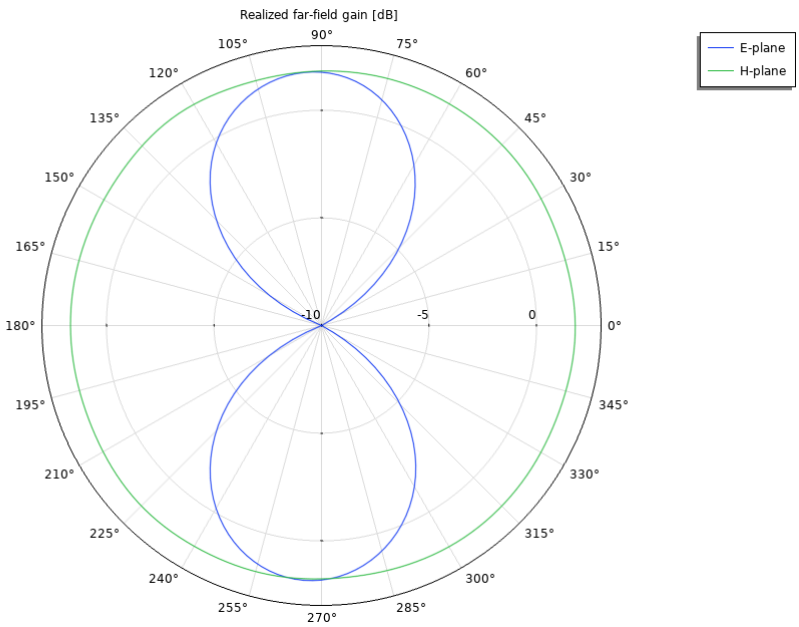

Figure 3.7: Realized far-field gain (E and H planes)

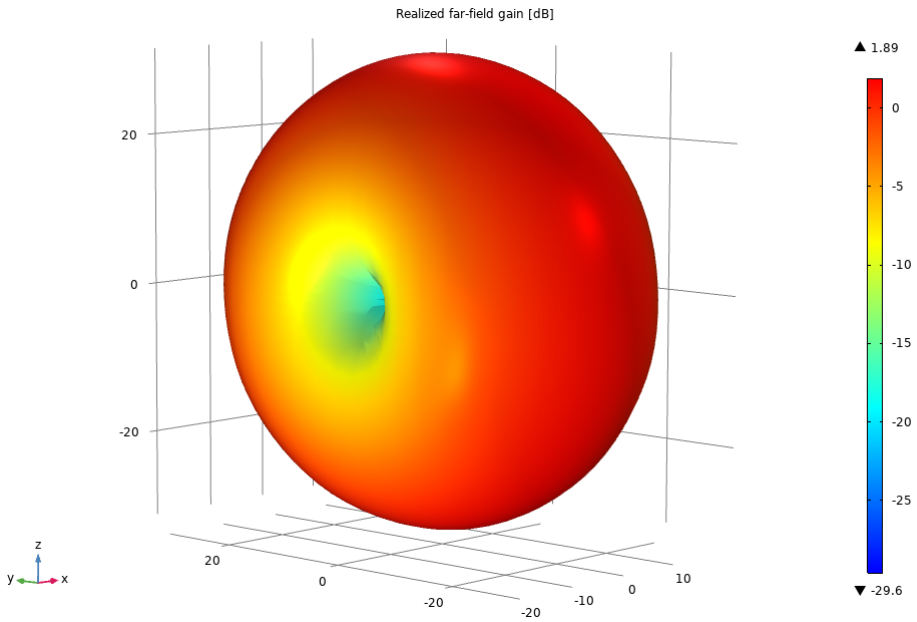

Figure 3.8: Realized far-field gain (3D)

The radiation patterns result slightly asymmetrical because the feed presence alters the antenna symmetry. The maximum realized gain is lower because of the balun transition losses. Figure 3.9 shows the feeding network alone simulation. At 140 GHz the s_{21} parameter is $-0.835dB$.

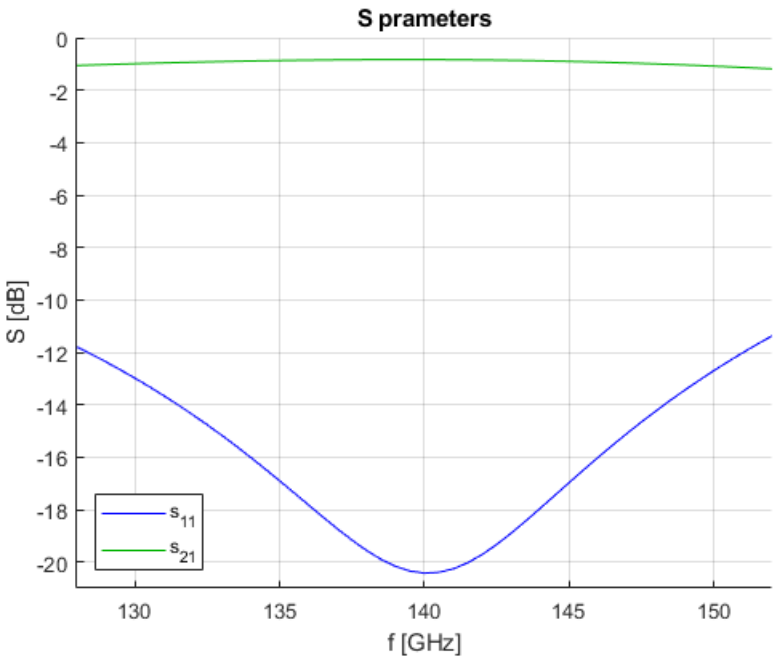

Figure 3.9: Feeding network S parameters

3.4 Lens models

3.4.1 Bowtie antenna combined with a multi-layer lens

Before the final lens design, the first step consists in the realization of a model with a lens composed by different dielectric material layers as shown in figure 3.10.

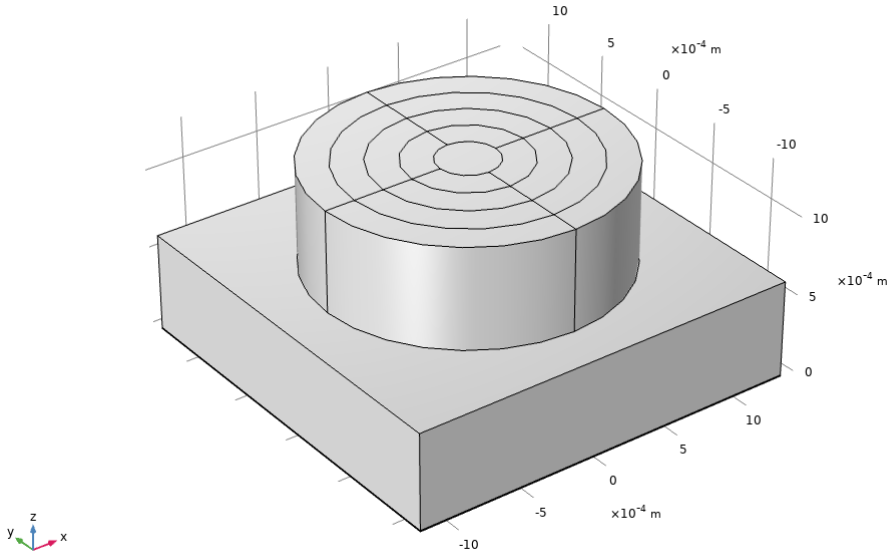

Figure 3.10: Multi-layer lens model in COMSOL

The lens is modelled as a cylinder with different dielectric circular layers placed above a spacer made of high resistive silicon substrate. The dielectric permittivity value of each layer is determined by equation 3.1 as it will be explained in chapter 4.1.

$$\varepsilon_r = \varepsilon_{min} + (\varepsilon_{max} - \varepsilon_{min}) \left(x \frac{w_{layer}}{r_{lens}} \right)^{\nu} \qquad with\ x = 1, 2, 3, 4, 5 \tag{3.1}$$

This structure is excited by the radiation of a bowtie antenna (the same discussed in the section 3.3.1) placed under the silicon spacer.

An optimization process is needed in order to obtain the best realized gain. This result is obtained by evaluating the return loss at the port and the realized gain in the z-direction trough a parametric sweep and choosing the best values. The degree of freedom considered are the lens height and radius and the spacer height. The best results are listed in the table below.

Parameters	**Value**
Lens height	679 μm
Lens radius	1015 μm
Spacer height	663 μm

The resulted radiation patterns, shown in figures 3.11 and 3.12, prove that the maximum realized gain is highly increased in the z direction, thanks to the lens presence.

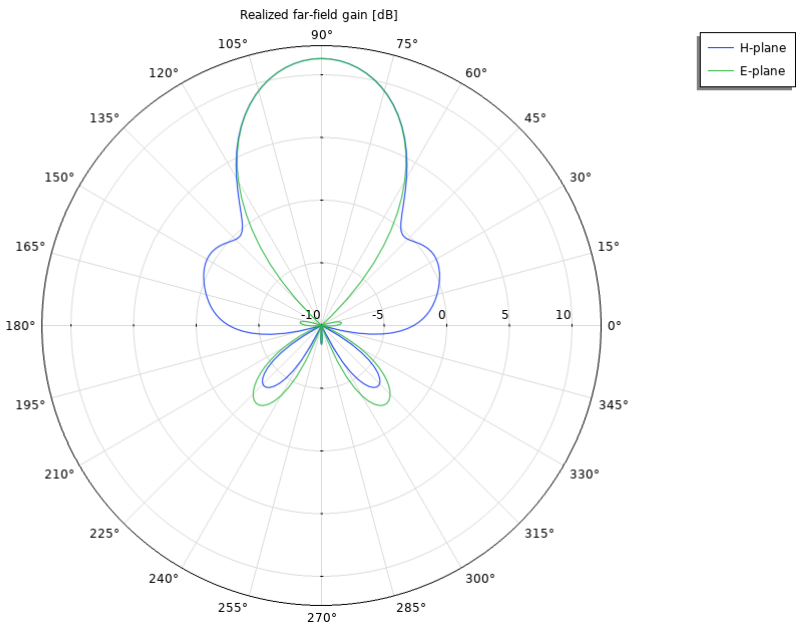

Figure 3.11: Realized far-field gain (E and H planes)

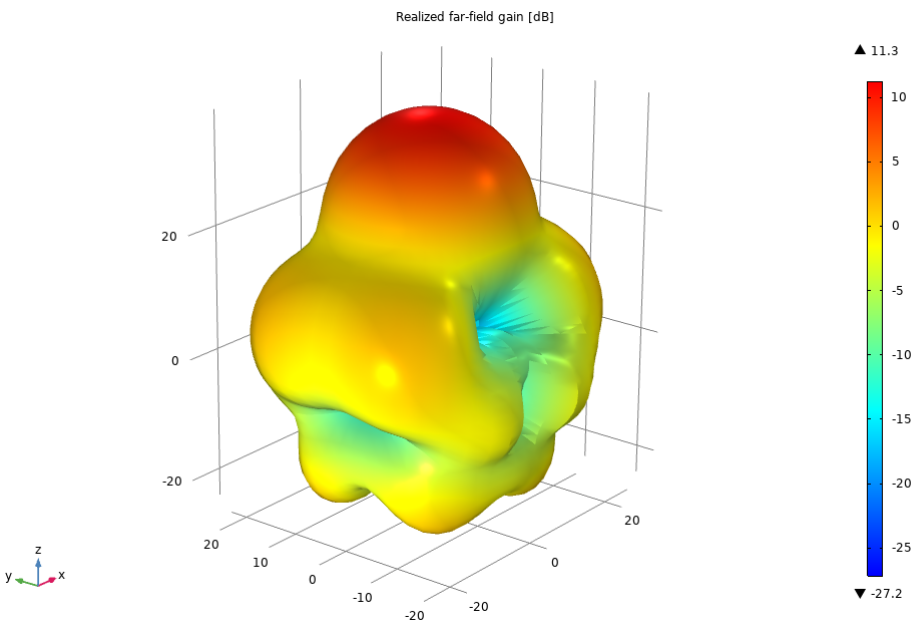

Figure 3.12: Realized far-field gain (3D)

3.4.2 Bowtie antenna combined with metamaterial lens

The next step consists in using the metamaterial instead of the different dielectric layers. The idea of the metamaterial is to obtain the desired dielectric permittivity value creating holes in the silicon cylinder substrate. If the holes have a dimension lower than the wavelength the electromagnetic incident wave sees a dielectric with a relative permittivity between the air and

the silicon value. The effective permittivity depends on the hole and silicon surfaces ratio. Figures 3.13 and 3.14 show the final lens design pattern.

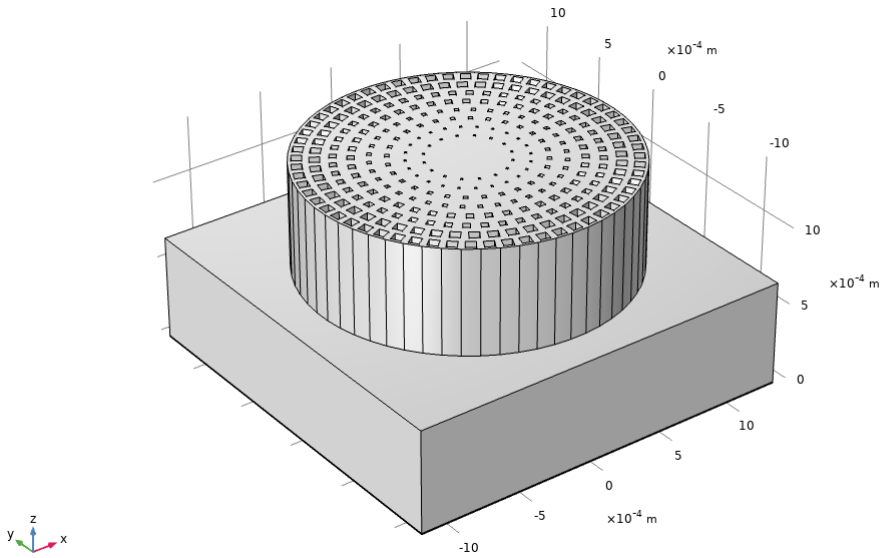

Figure 3.13: Metamaterial lens model in COMSOL

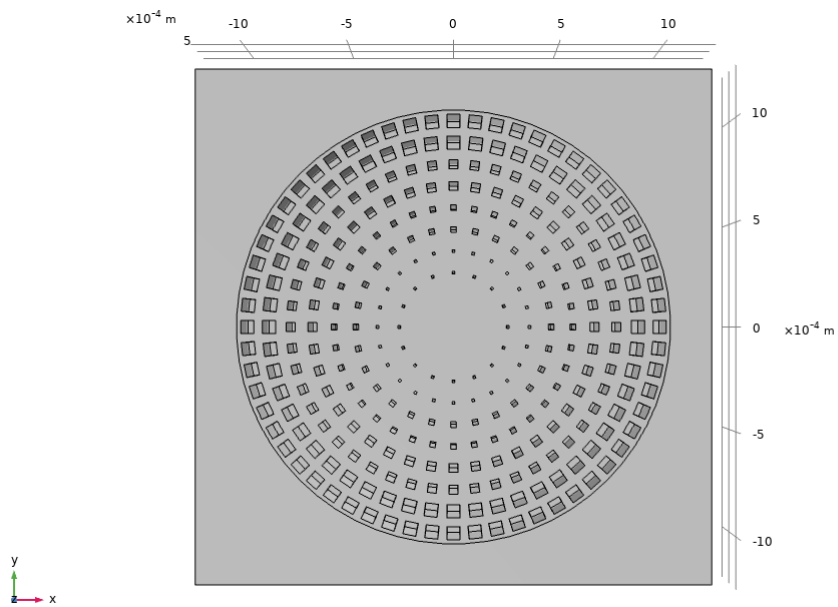

Figure 3.14: Top view of the metamaterial lens

The lens presents five different layers, the same as the previous model. Each layer has two rows of square holes with a dimension given by formula 3.2. The ε_r value is obtained by the

formula 3.1 proposed in section 3.4.1.

$$\frac{d_{holes}}{w_{layer}} = 1 - \frac{\varepsilon_r(x) - 1}{\varepsilon_{max} - 1} \tag{3.2}$$

The lens is placed above the bowtie antenna proposed in section 3.3.2. The model presents a high return loss value because of the feeding network presence. Although the radiation pattern remains still similar to the previous model, the high s_{11} value reduces the maximum realized gain. Hence a further optimization is needed. The optimum values, obtained by a sweep of the feeding network parameters, are listed in the table below.

Parameters	**Value**
Feed length	220 μm
Feed width	32 μm
Balun length	110 μm
Microstrip width	5 μm

Figures 3.15 and 3.16 show the radiation pattern after the optimization process. As shown, the maximum value is lower than the model presented in the previous section and the symmetry is lost due to the feeding network presence. The results are fully commented in chapter 4.

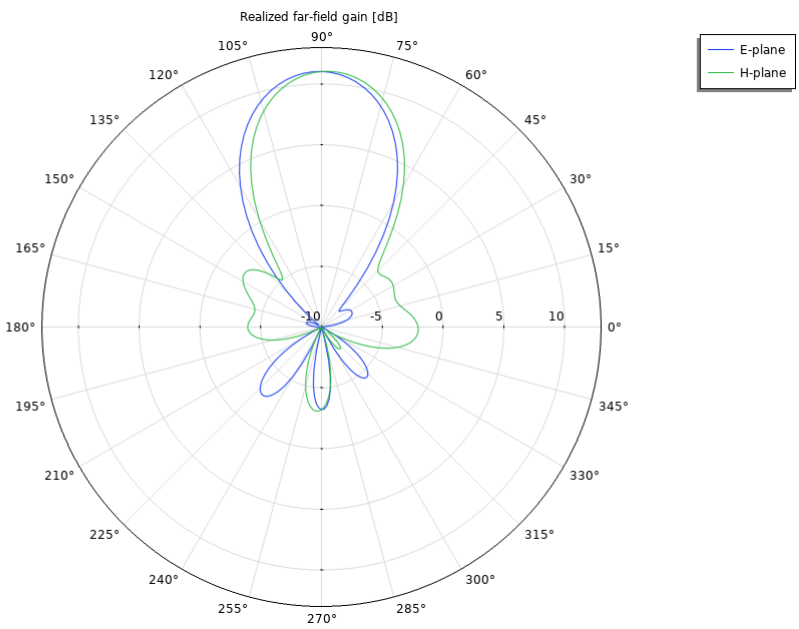

Figure 3.15: Realized far-field gain (E and H planes)

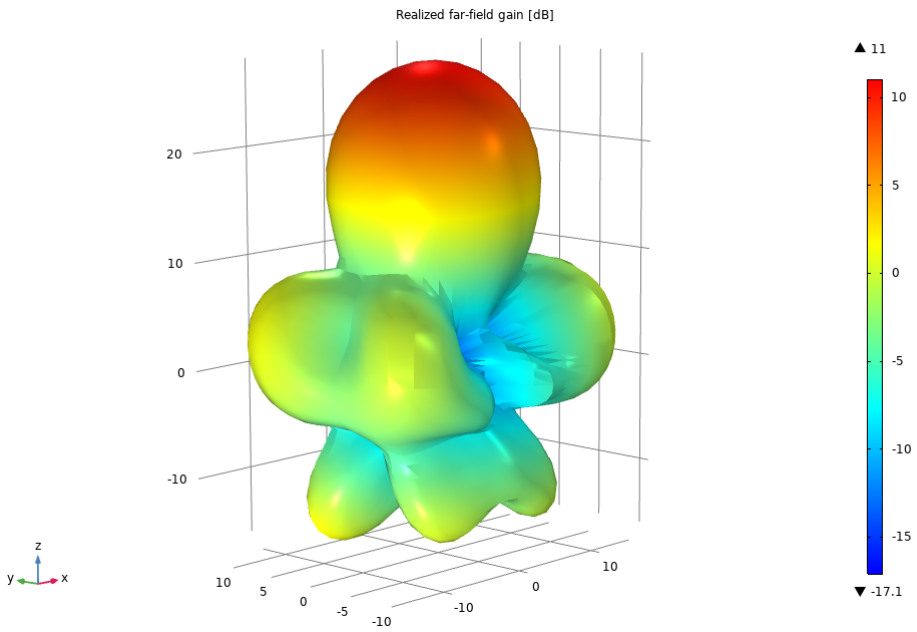

Figure 3.16: Realized far-field gain (3D)

Chapter 4

Results

Contents

4.1 Metamaterial lens dielectric permittivity and group velocity

An antenna placed on a dielectric material radiates the most energy in the dielectric direction due to the higher ε_r value than the air one. A classical dielectric lens collects the major part of the radiated energy and thanks to its curved profile makes it converge to the center enhancing the antenna directivity.

The metamaterial lens is a silicon cylinder divided in different circular layers. Each of them presents square holes with different dimensions. The holes dimension is much smaller than the electromagnetic wavelength in silicon which is $\lambda = 626\ \mu m$ at 140 GHz. An incident electromagnetic wave, that passes through the lens, behaves as if each layer is a different material with a different ε_r value. A variable ε_r means a variable group velocity (v_g) which implies different propagation speeds of the electromagnetic waves along the lens radius direction. The different propagation speeds due to the different ε_r values make the electromagnetic waves refract and converge in the lens center increasing the bowtie directivity.

Figures 4.1 and 4.2 represent the ε_r value and the holes dimension depending on the considered layer. There are five layers in the lens structure. The outer layer has the biggest holes and it has $\varepsilon_r = 6.5$, the inner has no holes and it has $\varepsilon_r = 11.7$ the same value of the silicon.

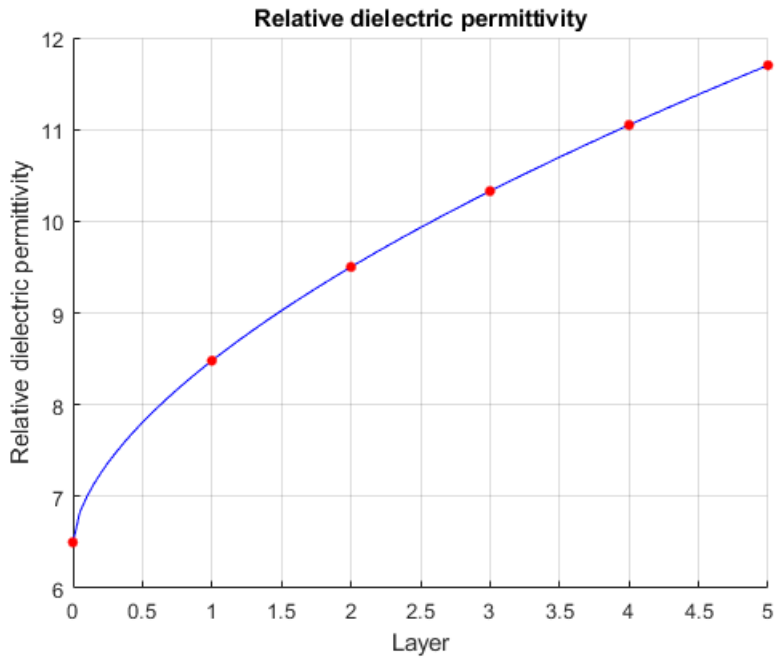

Figure 4.1: Dielectric constant value for each layer (ε_r)

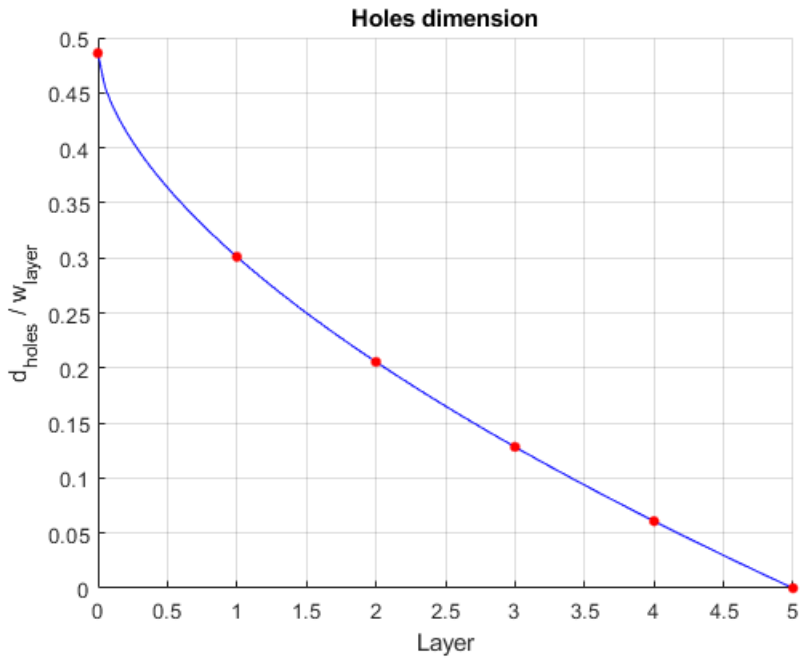

Figure 4.2: Holes dimension for each layer

The ε_r value and the holes dimension in proportion to the layer width for each x layer is obtained by the following formulae:

$$\varepsilon_r = \varepsilon_{min} + (\varepsilon_{max} - \varepsilon_{min}) \left(x \frac{w_{layer}}{r_{lens}} \right)^{\nu} \tag{4.1}$$

$$\frac{d_{holes}}{w_{layer}} = \frac{1 - (\varepsilon_{min} + (\varepsilon_{max} - \varepsilon_{min}) \left(\left(x \frac{w_{layer}}{r_{lens}} \right)^{\nu} \right) - 1)}{(\varepsilon_{max} - 1)} \tag{4.2}$$

Parameters	**Value**
ε_{max}	11.7
ε_{min}	6.5
d_{holes}/w_{layer}	5
ν	0.6

4.2 Planar bowtie antenna

4.2.1 Bandwidth

Figure 4.3 shows the bowtie antenna s_{11} simulation results from 128 GHz to 152 GHz. The plot shows a minimum at 141 GHz and a return loss value of -26 dB at working frequency (140 GHz). The bandwidth which is determined by the -10 dB threshold is 20 GHz. As expected the bowtie antenna has a broadband characteristic with a band of 14.3%.

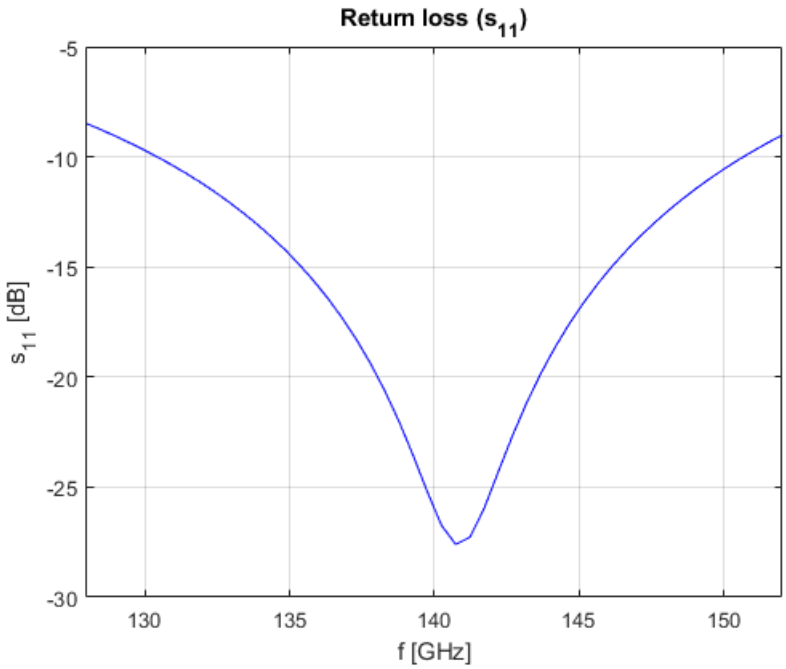

Figure 4.3: Bowtie return loss (s_{11})

4.2.2 Radiation pattern

Figures 4.4 and 4.5 show the radiation pattern simulation results at 140 GHz, for $\phi = 0°$ (E plane) and $\phi = 90°$ (H plane).

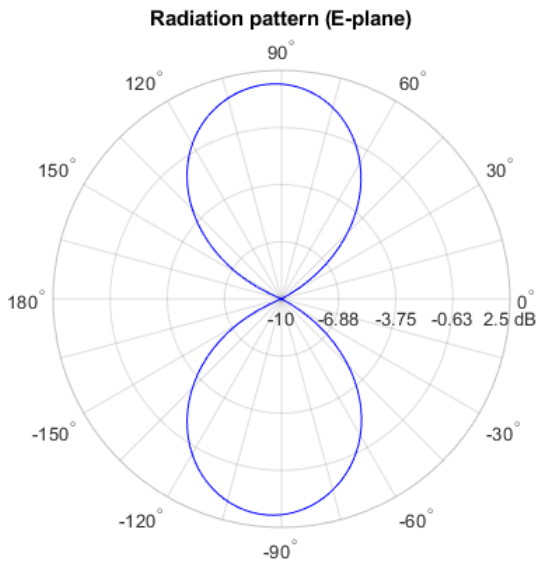

Figure 4.4: Bowtie radiation pattern (E-plane)

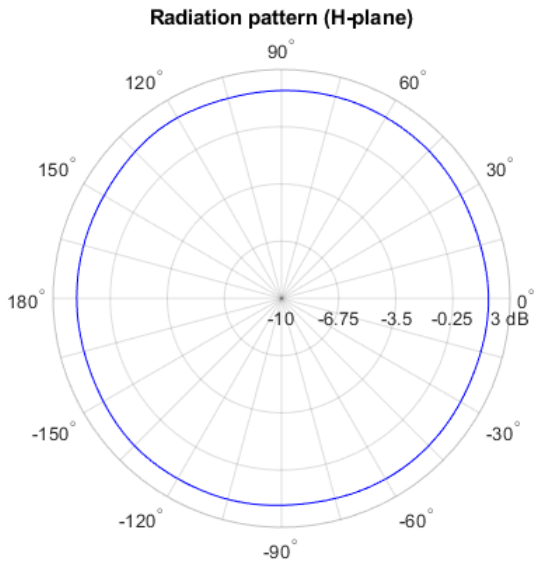

Figure 4.5: Bowtie radiation pattern (H-plane)

These plots represent the realized far field gain at every θ. In the E plane the radiation pattern shows the presence of two zeros at 0° and 180° respectively with a null to null beam width of 180°. In the H plane the radiation is almost omnidirectional. The highest gain in this plane is not in the z-direction but at $\theta \approx 115°$. In both the figures the radiation patter is not symmetrical. This is due to the asymmetrical network used to feed the antenna. The maximum realized gain is $G_r = 1.89$ dB. The radiation efficiency is $e_r = 85.01\%$ and the total efficiency of $e_{tot} = 84.83\%$.

4.2.3 Realized gain

Figure 4.6 shows the maximum bowtie antenna realized gain in the frequency range 128/152 GHz. As it shown, the maximum value is $G_r = 1.89$ dB at working frequency (140 GHz) and it monotonically decrease for lower and higher frequency value.

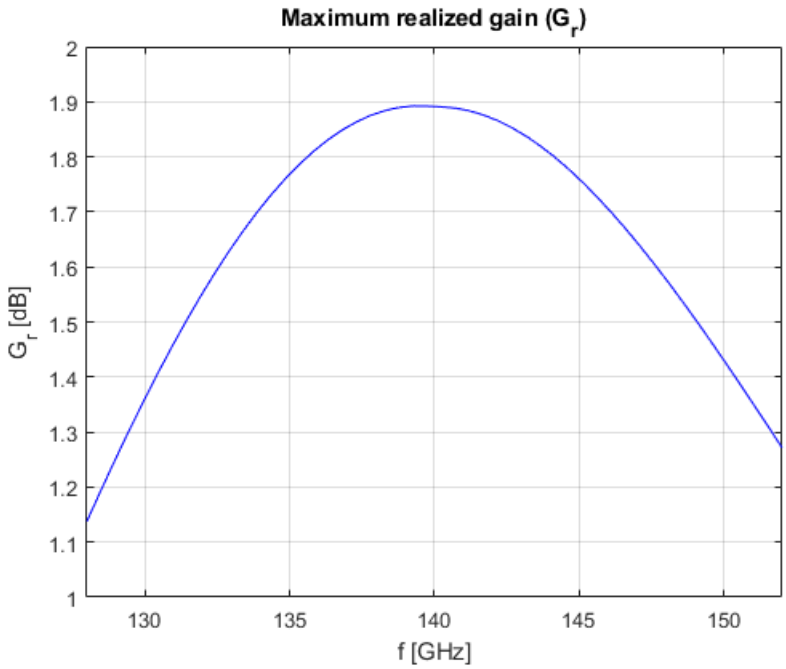

Figure 4.6: Bowtie realized gain (G_r)

4.3 Planar bowtie antenna combined with metamaterial lens

4.3.1 Bandwidth

Figure 4.7 shows the s_{11} simulation result from 128 GHz to 152 GHz. The bandwidth of the bowtie antenna combined with the lens at the threshold of -10 dB is 14 GHz. The presence of the metamaterial lens reduces the band of the bowtie antenna, but it remains a 10% band, which is fairly broad. At 140 GHz the return loss has a value of -22 dB.

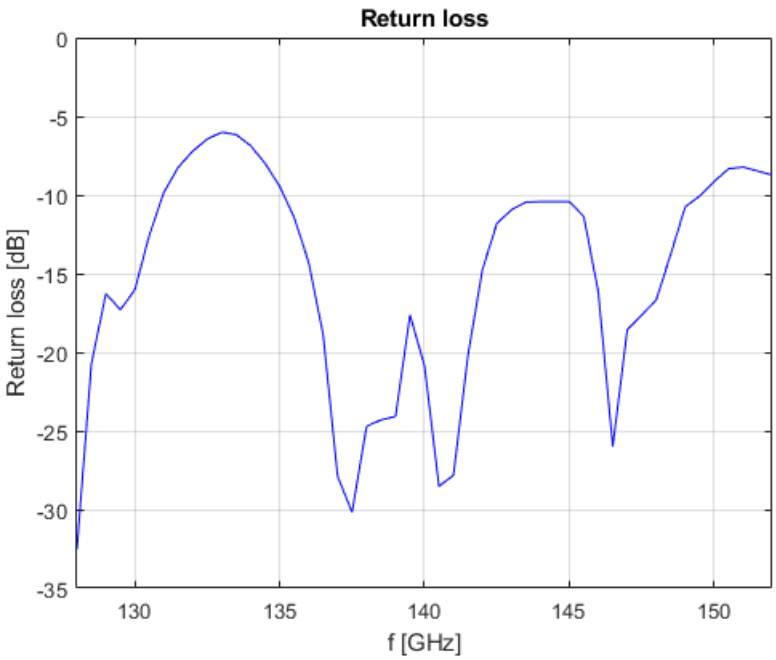

Figure 4.7: Bowtie combined with metamaterial lens return loss (s_{11})

4.3.2 Radiation pattern

Figures 4.8 and 4.9 show the radiation pattern simulation results at 140 GHz, for $\phi = 0°$ (E plane) and $\phi = 90°$ (H plane).

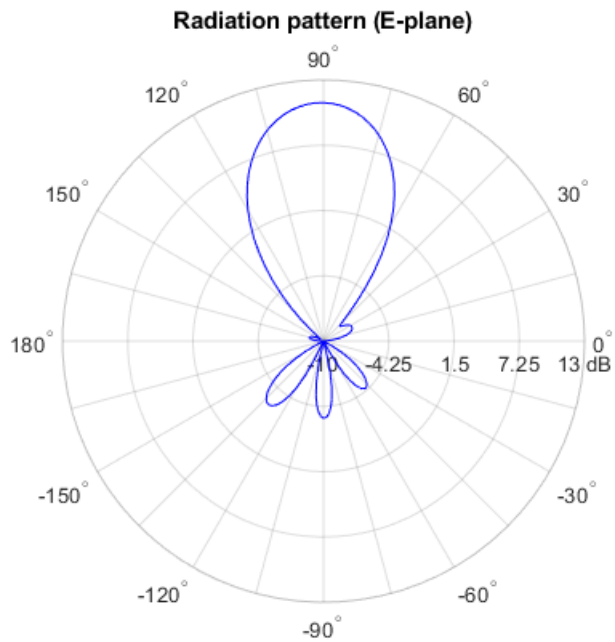

Figure 4.8: Bowtie combined with metamaterial lens radiation pattern (E-plane)

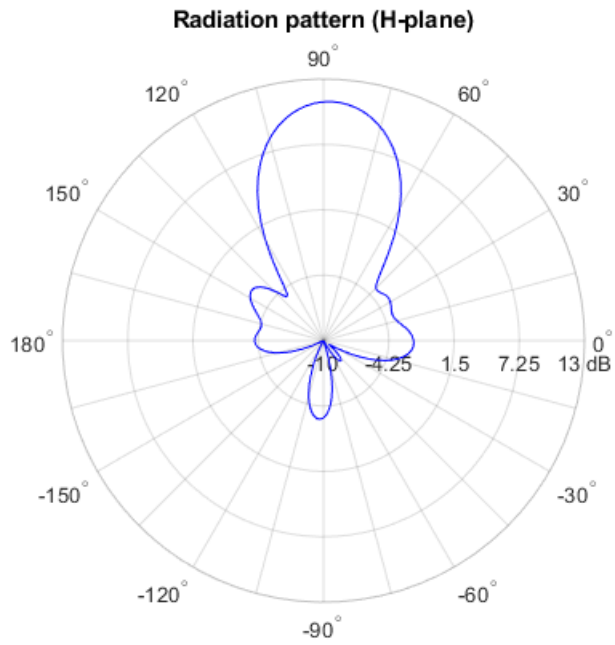

Figure 4.9: Bowtie combined with metamaterial lens radiation pattern (H-plane)

These plots represent the realized far field gain at every θ obtained by a 3D simulation of the bow-tie antenna combined with a metamaterial lens. The maximum realized gain value is $G_r = 11.02$ dB. The radiation efficiency is $e_r = 82.37\%$ and the total efficiency is $e_{tot} = 81.70\%$. These results show that the lens had highly increased the gain and the directivity of the antenna in both the E and H planes.

4.3.3 Realized gain

The realized gain varies in frequency as shown in figure 4.10. In the bandwidth range it goes from 5/6 dB at boundary frequency to 11 dB at 140 GHz. However, the bowtie combined with lens realized gain value is higher than the bowtie alone. With the increasing frequency (especially after 146 GHz) the radiation pattern starts to change from the designed one. The maximum realized gain direction is not directed in $\theta = 0°$ anymore. On the other side with the decreasing frequency the maximum gain direction remains the same.

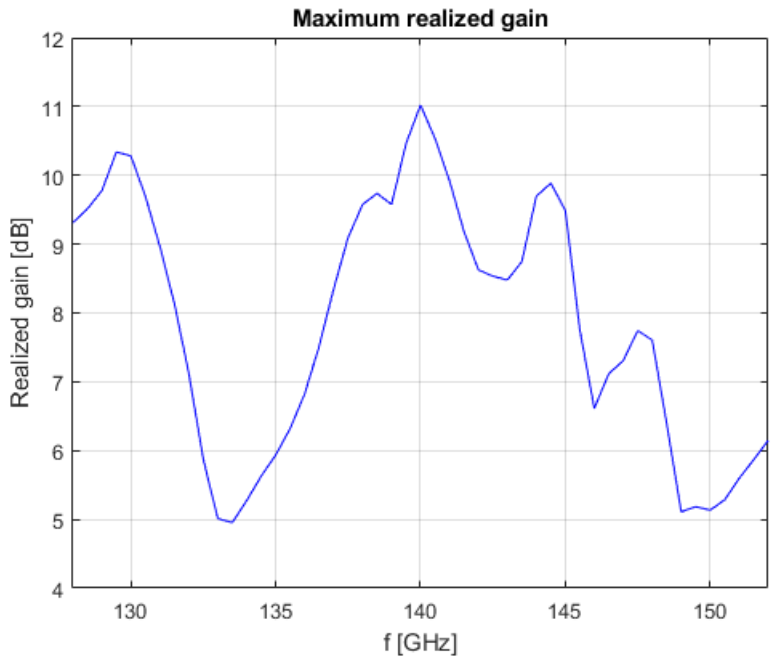

Figure 4.10: Bowtie combined with metamaterial lens realized gain (G_r)

Conclusion

This thesis had the objective to present a design for a cylindrical gradient index lens using metamaterials to improve antenna gain. According to simulations, as reported in chapter 4, the antenna combined with the metameterial lens presents a realized gain of 11 dB at 140 GHz. This value is over five times higher than the 1.89 dB gain of the bowtie alone. The final design can be printed using IHP SiGe technology. This allows to realize the lens in the same productive process of the antenna. Even if simulations give reasonable results, empirical measurements are required in order to validate the data obtained by the models. This metamaterial lens can represent a valid solution to enhance gain and it can be used with other kind of antennas or even arrays.

References

[1] Richard W. Ziolkowski Nader Engheta. "Metamaterials: Physics and Engineering Explorations". In: Wiley-IEEE Press, 2006. Chap. 1. ISBN: 978-0-471-76102-0.

[2] R.W. Ziolkowski and Ehud Heyman. "Wave Propagation in Media Having Negative Permittivity and Permeability". In: *Physical review. E, Statistical, nonlinear, and soft matter physics* 64 (Dec. 2001), p. 056625. DOI: 10.1103/PhysRevE.64.056625.

[3] D. R. Smith et al. "Gradient index metamaterials". In: *Phys. Rev. E* 71 (3 Mar. 2005), p. 036609. DOI: 10.1103/PhysRevE.71.036609. URL: https://link.aps.org/doi/10.1103/PhysRevE.71.036609.

[4] Josep Canet-Ferrer. "Metamaterials and Metasurfaces". In: IntechOpen, 2019. Chap. 4. ISBN: 978-1-789-84842-7.

[5] Yuandan Dong and Tatsuo Itoh. "Metamaterial-Based Antennas". In: *Proceedings of the IEEE* 100.7 (2012), pp. 2271–2285. DOI: 10.1109/JPROC.2012.2187631.

[6] Rui Yang, Wenxuan Tang, and Yang Hao. "A broadband zone plate lens from transformation optics". In: *Optics express* 19 (June 2011), pp. 12348–55. DOI: 10.1364/OE.19.012348.

[7] Oscar Quevedo-Teruel et al. "Transformation optics for antennas: Why limit the bandwidth with metamaterials?" In: *Scientific reports* 3 (May 2013), p. 1903. DOI: 10.1038/srep01903.

[8] E.W. Marchand. *Gradient Index Optics*. Academic Press, 1978. ISBN: 9780124707504. URL: https://books.google.it/books?id=GBpRAAAAMAAJ.

[9] R.K. Luneburg and M. Herzberger. *Mathematical Theory of Optics*. University of California Press, 1964. ISBN: 9780520328266. URL: https://books.google.it/books?id=-t4bLCrwf60C.

[10] Benjamin Fuchs et al. "Design and Characterization of Half Maxwell Fish-Eye Lens Antennas in mm-Waves". In: *Microwave Theory and Techniques, IEEE Transactions on* 54 (July 2006), pp. 2292–2300. DOI: 10.1109/TMTT.2006.875255.

[11] Bo Hu et al. "A Novel Metamaterial-Based Planar Integrated Luneburg Lens Antenna With Wide Bandwidth and High Gain". In: *IEEE Access* 8 (2020), pp. 4708–4713. DOI: 10.1109/ACCESS.2019.2960634.

[12] Sang-Hoon Kim. *Generalized Eaton Lens at Arbitrary Refraction Angles*. 2011. arXiv: 1109.3977 [physics.optics].

[13] Jose-Manuel Poyanco et al. "3D-printed Wideband Hyperbolic Lens Antenna for Ka-band". In: *2020 14th European Conference on Antennas and Propagation (EuCAP)*. 2020, pp. 1–5. DOI: 10.23919/EuCAP48036.2020.9135878.

[14] José-Manuel Poyanco, Francisco Pizarro, and Eva Rajo-Iglesias. "3D-printed dielectric GRIN planar wideband lens antenna for 5G applications". In: *2021 15th European Conference on Antennas and Propagation (EuCAP)*. 2021, pp. 1–4. DOI: 10.23919/EuCAP51087.2021.9411342.